2021 43rd Annual International Conference of the
IEEE Engineering in Medicine & Biology Society (EMBC)
Oct 31 - Nov 4, 2021. Virtual Conference

A Treatise on Electrode Carrier Dislocation in Visual Prosthetic Devices

Diego Lujan Villarreal, Emilio José Cabezas Zevallos, Ana Marie Perea Del Ángel and Wolfgang H. Krautschneider, *Member, IEEE*

***Abstract*— Visual implants electrically activate adjacent neurons to induce artificial perception for visual impairment patients to restore some sight. Proximity of electrode carrier to the ganglion cell has attracted careful consideration due to its implications on secure electrochemical and single-localized stimulation. In this study, we postulate a novel strategy to treat the proximity of electrode-cell. A simulation framework includes the carrier dislocation using the geometric parameters of Argus II® epiretinal electrode carrier design. Lastly, we present results on the offset angle of displacement.**

***Clinical Relevance*— This postulates a novel strategy to treat the dislocation of electrode carrier confined with a single tack.**

I. Introduction

Retinal prostheses are designed to deliver prosthetic vision through electrical stimulation of the preserved neurons in the retina via subretinal or epiretinal electrodes when degenerative pathology is present, specifically age-related macular degeneration or retinitis pigmentosa. To date, distinct research groups have developed retinal implants [1-6] and latest clinical trials have reported sensations of visible symbols and shapes of light while the retina is electrically activated [4,5,7], hence validating the immense potential in visual amendment. Among fabricated epiretinal implants, Argus II reported a best measured visual acuity of 20/1260 in 7 out of 30 patients [8,9]. Alpha IMS and AMS have been implanted in clinical trials, resulting in a best measured visual acuity of 20/546 in 2 out of 9 patients [10-12]. An ideal visual implant would mimic natural activity of ganglion cells (RGCs). Still, since types of RGC are located tightly adjacent to each other, electrode specificity is required to assure that only desired information is transmitted independently [13].

Epiretinal prostheses face challenges, e.g. adequate fixation of the electrode array to the retina [14]. Stimulation to the central region within ± 10° of eccentricity from the fovea is of utmost importance for critical functions, such as reading, driving and object recognition [15]. Hence, as an imposed solution, a single tack is used in most cases [1-3]. Argus I and II held in place the electrode array directly in contact with the retina with a single titanium tack that crosses the retina, choroid and sclera [1-3], and providing amply robust safety profile [16]. RGC-carrier proximity and electrode distribution act as variables for the resulting activation area that estimates the quantity of cells triggered and determine the size and shape of the phosphenes [17]. The threshold current that once injected across the electrodes controls the final regions of stimulation and triggers the propagation throughout the layers of tissue. As the distance to the electrode increases, the peak current becomes insufficient to spread an activation response [17] and higher stimulation thresholds are needed. As the electrode size increases, charge density reduces. Yet, larger activation area is produced, which in consequence could trigger the stimulation of undesirable localities and thereby reduce the focal activation [17]. As the electrode size decreases, charge density increases, resulting in tissue harm [17]. When not foreseen, electrode breakdown and adverse tissue reactions may be caused due to the power dissipation, water-voltage window and constant demand of higher charge density injection and thus producing irreversible Faradaic reactions [17].

Saccade propagation is influenced by shape properties while scanning visual objects and should be considered to mimic the natural vision supported by normal and smooth pursuit eye motions [18]. Close electrode-RGC proximity can be guaranteed by locating the carrier near the ganglionic boundary using a single microtack [1-3]. When close proximity is achieved, lower thresholds are required. Still, typical saccades at a rate of 2–3 times per second [19] can relocate the carrier in the vitreous cavity [20] and can impact RGCs stimulation [21]. Electrode-cell distance along with electrode geometry are important factors to notice for RGC stimulation [23]. The development of finite element simulations or programmable software analysis represents a clear path to improve the understanding of said topics. Yet, unrealistic techniques have been presented [17,22,24-26], showing the retina and eye as a rectangle, or depicting the carrier as a homogeneous flat surface that dislocates concentrically relating to the retina, certainly simplifying the simulation approach anatomically and physiologically, and causing the results to be unreliable for further retinal implant studies and applications in real-life scenario.

II. Materials and Methods

Let us consider that the electrode carrier represents a portion of a hollow spherical segment cut off by two pairs of parallel planes. A single retinal tack holds the carrier in position on one edge, letting its end edge to move freely in space, see Fig. 1(a), (in black). Electrode carrier dislocation is then defined as the effect of a sphere fixated by a single tack and its displacement as the radius increases, see Fig. 1(a), (in dark-yellow). Cell-electrode proximity is then larger for large sphere radius. The points (X_{i1},Y_{i1}) and (X_{i2},Y_{i2}) that define the location of the electrode carrier, see Fig. 1(b), are described by $(R\cos[(\pi-\theta)/2], R\sin[(\pi-\theta)/2])$ and $(-R\sin[\alpha], R\cos[\alpha])$,

Lujan V. D is with the Mechatronics Department at the Monterrey Institute of Technology and Higher Education (ITESM), 64849 Mexico (e-mail: diego.lujan@tec.mx). Cabezas Z. E. and Del Ángel P. A. are studying Biomedical Engineering at ITESM. Krautschneider W. is with the Institute for Integrated Circuits at the Hamburg University of Technology (e-mail: krautschneider@tuhh.de).

respectively. The distance running from the origin of the retina to the electrode carrier is defined as $R = \hat{R} + \Psi$, where $\hat{R} = r_r \cos[\kappa/2]$ and $\Psi = (L^2-L'^2)^{1/2}$, see Fig. 1(c). The angle between y-coordinate and the edge of the carrier is defined as $\alpha = \text{acos}(1-W^2/2R^2)$. We found that the expressions can be written by letting $L = 2r \sin(\xi/4)$, $L' = r \sin(\xi/2)$ and $W = 2r \sin(\beta/2)$. Sphere center points of the carrier $(X_1,Y_1,0)$ are obtained as

$$X_1 = \frac{X_{i2}+X_{i1}}{2} + \frac{Y_{i1}-Y_{i2}}{W}\sqrt{r^2-\frac{W^2}{4}}, \quad (1)$$

$$Y_1 = \frac{Y_{i2}+Y_{i1}}{2} + \frac{X_{i2}-X_{i1}}{W}\sqrt{r^2-\frac{W^2}{4}}. \quad (2)$$

The sphere offset angle of electrode carrier with respect to the sphere retinal coordinates, Fig. 1(a),(b), is calculated as

$$\zeta = \frac{1}{2}(\pi-\beta) - \text{atan}\left(\text{abs}\left(\frac{y_a}{X_1}\right)\right), \quad (3)$$

$$y_a = Y_1 - \left(Y_{i2} - X_{i2}\frac{Y_{i2}-Y_1}{X_{i2}-X_1}\right). \quad (4)$$

As for plotting the points of the electrode carrier, they can be described as $X_2 = X_1 + r \sin(\rho) \cos(\varphi)$, $Y_2 = Y_1 + r \sin(\rho) \sin(\varphi)$, $Z_2 = r \cos(\rho)$ with values inside the electrode carrier space $\{\varphi \mid \zeta + (\pi-\beta)/2 \le \varphi \le \zeta + (\pi+\beta)/2\}$ and $\{\rho \mid (\pi-\xi)/2 \le \rho \le (\pi+\xi)/2\}$. The proximity of electrode carrier to the surface of the retina is obtained as $P = [(X_R-X_2)^2+(Y_R-Y_2)^2+(Z_R-Z_2)^2]^{1/2}$, where (X_2,Y_2,Z_2) are points within the electrode carrier space where electrodes are located $X_2 = X_1 + r \sin(\xi_0) \cos(\beta_0)$, $Y_2 = Y_1 + r \sin(\xi_0) \sin(\beta_0)$, and $Z_2 = r \cos(\xi_0)$ and letting the z-coordinate offset of the electrode carrier sphere as zero. We found that the angles β_0 and ξ_0 can be defined as

$$\beta_0 = \zeta + \frac{1}{2}(\pi-\beta) + \text{acos}\left(1-\frac{\Delta w^2}{2r^2}\right), \quad (5)$$

$$\xi_0 = \frac{1}{2}(\pi-\xi) + \text{acos}\left(1-\frac{\Delta l^2}{2r^2}\right), \quad (6)$$

with values within the electrode carrier space $\{\Delta w \mid 0 \le \Delta w \le w\}$ and $\{\Delta l \mid 0 \le \Delta l \le l\}$. The intersection of a parametric line from the center of electrode carrier sphere and normal to the electrode carrier space and the surface of the retina is given by $X_R = X_1 + u(X_2-X_1)$, $Y_R = Y_1 + u(Y_2-Y_1)$ and $Z_R = uZ_2$, by letting the z-coordinate offset as zero. u is defined as

$$u = \begin{cases} \text{if } Y_R<0, & \frac{1}{2a}\left(-b-\sqrt{b^2-4ac}\right) \\ \text{otherwise,} & \frac{1}{2a}\left(-b+\sqrt{b^2-4ac}\right) \end{cases}, \quad (7)$$

with values a, b, and c of a quadratic equation of the form of $au^2 + bu + c = 0$,

$$a = (X_2-X_1)^2+(Y_2-Y_1)^2+Z_2^2, \quad (8)$$

$$b = 2[X_1(X_2-X_1)+Y_1(Y_2-Y_1)], \quad (9)$$

$$c = X_1^2+Y_1^2-r_r^2. \quad (10)$$

As for the electrode carrier space, the suitable equations define the angles $\Delta\Omega_x$ and $\Delta\Omega_y$ for printing separately the electrodes,

$$\Delta\Omega_x = \zeta + \frac{1}{2}(\pi-\beta) + \text{acos}\left[1-\frac{(\Delta w+r_e \sin\Omega)^2}{2r^2}\right], \quad (11)$$

$$\Delta\Omega_y = \frac{1}{2}(\pi-\xi) + \text{acos}\left[1-\frac{(\Delta l+r_e \cos\Omega)^2}{2r^2}\right], \quad (12)$$

which describe that, along the surface of the electrode carrier, the circular electrode with center $(\Delta w, \Delta l)$, electrode radius r_e and the set of real numbers $\{\Omega \mid 0 < \Omega \le 2\pi\}$ are the locus of angles $(\Delta\Omega_x, \Delta\Omega_y)$. The points of the circular electrode printed on the electrode carrier can be parametrized by means of

$$\Omega_x = X_1 + r \sin(\Delta\Omega_y) \cos(\Delta\Omega_x), \quad (13)$$

$$\Omega_y = Y_1 + r \sin(\Delta\Omega_y) \sin(\Delta\Omega_x), \quad (14)$$

$$\Omega_z = r \cos(\Delta\Omega_y). \quad (15)$$

Angles β, ξ, θ, and κ are defined in table 1. A Matlab (MathWorks, Inc., United States, Version 7.13) script implemented the carrier dislocation. The technology of the epiretinal electrode carrier of Argus II® was used, which includes a single retinal tack on one edge of the carrier and 60 electrodes of 200 μm of diameter [1-3]. Note that the equations hold for any given carrier fixed with a single tack.

III. Results and Discussion

Spherical radius of the carrier is the most significant parameter for realizing electrode dislocation which shifts the center of its sphere to the fourth quadrant, i.e. (*x*,-*y*), see Fig. 1(a), (b). For assuring mathematical simplicity, the carrier's sphere *z*-coordinate offset was set to zero, producing a vertical reflection across the *y-axis*, see Fig. 1(c). When dislocation arises, the carrier lifts off from the retinal surface and follows the axis normal to the retina where a single retinal tack holds in position with an angle of $(\pi-\theta)/2$, see Fig. 2(a), 3(a). For reassuring a natural displacement, the corners of the carrier are forced to be in contact with the retinal surface, see Fig. 1(c). For testing our simulation framework, the proximity of electrode-retinal surface is evaluated for different spherical radius of dislocation of 15, 20, 40 and 100 mm, see Fig. 2(a). The maximum proximity was observed using a spherical radius of 100 mm around the center of the carrier reaching 1.2 mm. Body cells can be triggered with low stimulus intensities once the activating electrode is near to the retinal layer. As a result, specific areas of the retina are stimulated. To stimulate certain body cells as proximity increases, stimulus intensities must be increased. This induces variations in the stimulus volume due to the changing current spread to the ground electrode. Visual epiretinal devices are placed close to the retinal surface to provide low stimulation thresholds as well as a more specific triggering field [17,22]. Normal saccades at a rate of 2–3 times per second [19] can displace the electrode array in the vitreous cavity [20] and locate it with an angle, changing the direction of stimulus. As a result, RGC single stimulation would be affected. Evidence on computational simulation of RCG activation [27] suggest that a small offset

Fig. 1(a)

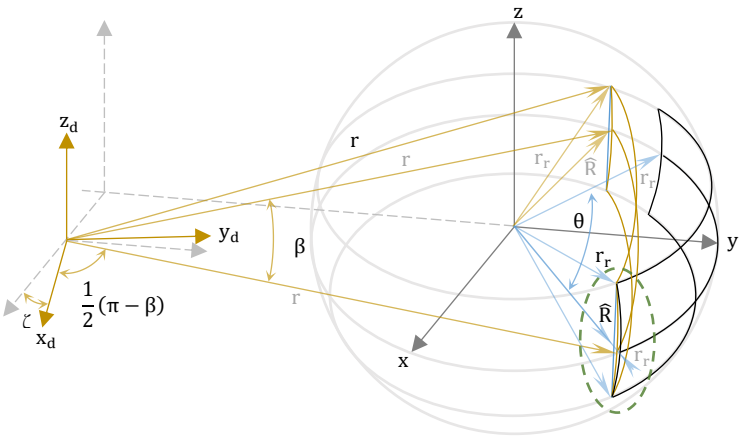

TABLE I. DESCRIPTION OF PARAMETERS

Par.	*Description*
(x,y,z)	Coordinates of retina
(x_d,y_d,z_d)	Coordinates of electrode carrier dislocation
r_r	Spherical radius of retina
w	Width of electrode carrier
l	Length of electrode carrier
r	Spherical radius of dislocation
β = w/r	Arc-width angle of dislocation seen from (x_d,y_d,z_d)
σ	Arc-width angle of dislocation seen from (x,y,z)
ξ = l/r	Arc-length angle of dislocation seen from (x_d,y_d,z_d)
ζ	Offset angle of electrode carrier dislocation
κ = l/r_r	Arc-length angle of dislocation seen from (x,y,z)
θ = w/r_r	Arc-width angle seen from (x,y,z)
α	Arc-width angle from y to the electrode carrier

Fig. 1(b)

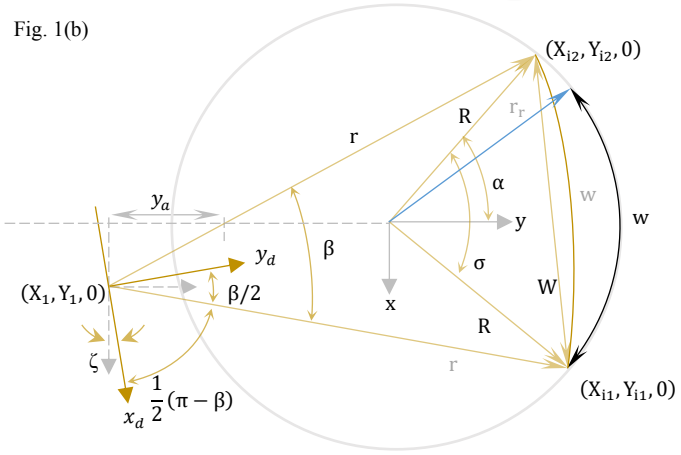

Fig. 1(c)

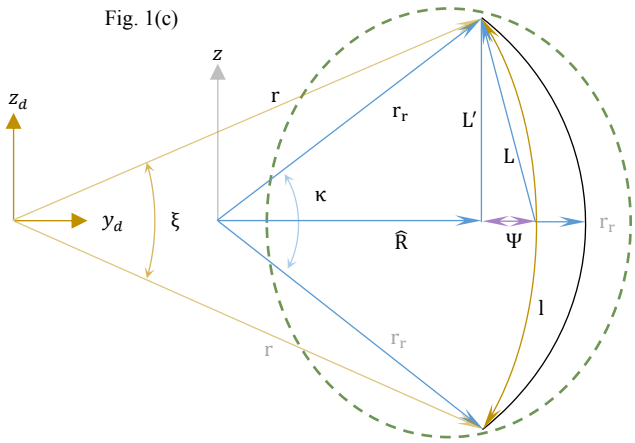

Figure 1. Electrode carrier dislocation seen in different views. Electrode carrier not drawn to scale.

angle of displacement of 2° and 4° with proximity of 200 µm was sufficient to alter the activation area produced byelectrode stimulation, delivering complex percepts e.g. an arc, triangle and an egg shape, (see Fig. 3(c) in [27]). Offset angle of displacement is vital since regions of electrode array may be closer to the target neurons and current spread may not produce a symmetrically stimulating field on the retina. This will cause changes in the stimulus region, resulting of percepts with shapes other than a "round" spots of light [27]. For testing, the offset angle of displacement is defined as the angle between the intersection of the tangent planes of the retina and the carrier surface at points of intersection through the center of electrodes, see Fig. 3(a) for clarification. The offset angles for an array of 60 electrodes are plotted for different spherical radius of dislocation of 15, 20, 40 and 100 mm, see Fig. 3(b). Row of electrodes is plotted on the *x-axis*. The columns are displayed inside the area of dislocation. Note the same colors for the rows 1st and 6th, 2nd and 5th, 3rd and 4th, which reflects a similar result due to the vertical reflection across the *y-axis*.

Evidence of focal proliferative vitreoretinopathy at the tack's fixation location implies the requirement for alternative epiretinal stimulator fixation procedures [28]. Evidence of the Argus® II interim report of the first 30-patients during the 6 months observation period showed two cases of retinal tack dislocation that required retacking. Hence, for systems that run leadwires from the vitreous via the sclera, there is also the possibility of mechanical injury to the retina and an elevated chance of inflammation [1]. Multiple mechanisms have been appointed to measure RGC-carrier distance, such as Optical Coherence Tomography (OCT) [3,20,29] and Fundus Photography [3]. Still, the principal cause of failure is severe nystagmus (uncontrolled eye movements) existing in the majority of blind subjects, which cause images and measurements to be unclear and unreliable [3]. Saccade frequency is constantly transitioning between the periods of visibility and invisibility and decreasing during prolonged fixation. Hence, eye movements can be determined as objective tools for evaluating the performance of retinal implants [22]. Recently [3], a poor signal-to-noise ratio (SNR) appeared in clinical trials due to opacity in various eye components of subjects, resulting in OCT images with unclear parameters. So, the number of subjects decreased and were unable to measure via imaging methods. Another factor to consider is the test times and procedures for imaging method. OCT involves a tracking algorithm which scans the eye for just a few minutes, ignoring the eye fatigue which could be critical in evaluating correct electrode-retina distance [3]. Therefore, mathematical approaches similar to this should be consider.

Retinal prostheses face significant challenges. A realistic restoration of typical RGC activity is projected to include specific and independent activation of solitary RGC forms. For single-localized stimulation, novel methods have been developed to constrain the volume region of stimulation to the volume of single RGCs [13,17,21,30]. Still, electrode array

Fig. 2(a)

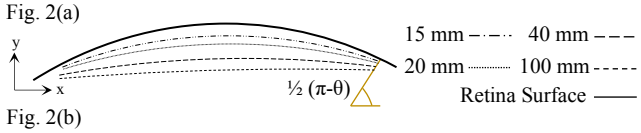

Fig. 2(b)

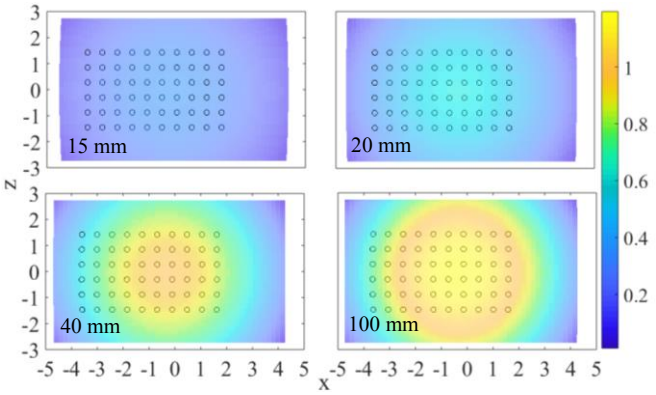

Figure 2. (a) Electrode carrier and (b) proximity for different spherical radius of dislocation. Units in millimeters.

Fig. 3(a)

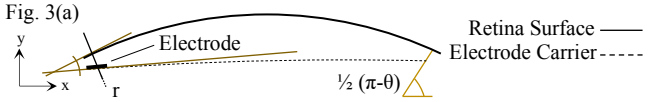

Fig. 3(b)

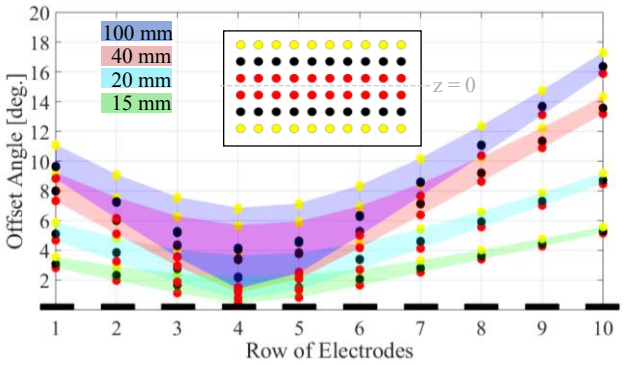

Figure 3. (a) Offset angle using tangential planes of spherical retina and electrode carrier at intersection points of electrodes. (b) Offset angle for different spherical radius of dislocation.

distribution and RGC-carrier distance continue as key factors for resolution patterns originated by neurological activity and perceptive stimulation that determines the response of RGCs.

IV. Conclusion

Because of the consequences for safe electrochemical and independent-localized stimulation, the proximity of the electrode carrier to the RGC has received detailed attention. In this report, we propose an innovative technique for treating electrode-cell proximity. Carrier dislocation is simulated using the geometric parameters of the Argus II® epiretinal electrode carrier design.

References

[1] K.S. Robert, et al. Visual prostheses for the blind, Trends in Biotechnology, Volume 31, Issue 10, 2013, Pages 562-571

[2] Second Sight Medical Products. Argus II® Retinal Prosthesis System Surgeon Manual. 2013. Available from https://www.accessdata.fda.gov/cdrh_docs/pdf11/h110002c.pdf Accessed April 16, 2021

[3] A. K. Ahuja, et al. Factors Affecting Perceptual Threshold in Argus II Retinal Prosthesis Subjects. Trans. Vis. Sci. Tech. 2013;2(4):1.

[4] M. Keseru, et al. Acute electrical stimulation of the human retina with an epiretinal electrode array. Acta Ophthalmol. 90, e1 –e8 (2012)

[5] S. Klauke, et al.: Stimulation with a wireless intraocular epiretinal implant elicits visual percepts in blind humans. In. Op. Vis. Sci. 52, 449–455 (2011)

[6] R Eckhorn, et al. Visual resolution with retinal implants estimated from recordings in cat visual cortex. V. Res. 2006 Sep;46(17):2675-90.

[7] M.S. Humayun. Visual perception in a blind subject with a chronic microelectronic retinal prosthesis. Vision Res. 43, 2573–2581 (2003)

[8] H Stronks. et al. "The functional performance of the Argus II retinal prosthesis" Expert Review of Med Dev, vol. 11, nº 1, pp. 23-30, 2014.

[9] A. C. Ho, et al. "Long-Term Results from an Epiretinal Prosthesis to Restore Sight to the Blind" Opht, vol. 122, nº 8, pp. 1547-1554, 2015.

[10] L. N. Ayton, et al. "An update on retinal prostheses" Clinical Neurophysiology, vol. 131, nº 6, pp. 1383-1398, 2020.

[11] T. L. Edwards, et al. "Assessment of the electronic retinal implant alpha AMS in restoring vision to blind patients with end-stage retinitis pigmentosa" Opht, vol. 125, nº 3, pp. 432-443, 2018.

[12] E. Bloch, et al. "Advances in retinal prosthesis systems" Therapeutic advances in ophthalmology, vol. 11, pp. 1-16, 2019.

[13] LH Jepson, et al. Spatially Patterned Electrical Stimulation to Enhance Resolution of Retinal Prostheses. J . 2014 Apr 2;34(14):4871– 4881.

[14] N. Gregori, et al. "Retinal anatomy and electrode array position in retinitis pigmentosa patients after Argus II implantation: an international study" Ame J of Oph, vol. 193, pp. 87-99, 2018.

[15] Nelson P, et al. Quality of life in glaucoma and its relationship with visual function. J Glaucoma. 2003 Apr;12(2):139–150.

[16] Y. H. L. Luo, et al. "The Argus® II retinal prosthesis system" Progress in retinal and eye research, vol. 50, pp. 89-107, 2016

[17] D. L. Villareal, et al. "A Treatise of the Physical Aspects of Phosphenes and Single-Cell Selectivity in Retinal Stimulation" Int J of Computational & Neu Eng, vol. 4, nº 2, pp. 55-70, 2017.

[18] N. Paraskevoudi, et al. "Eye movement compensation and spatial updating in visual prosthetics: mechanisms, limitations and future directions" Frontiers in systems neuroscience, vol. 12, p. 73, 2019.

[19] Freeman, D.K., et al. Encoding visual information in retinal ganglion cells with prosthetic stimulation. J. Neural Eng. 8, 035005 (2011) 19.

[20] De Balthasar, C., et al. Factors affecting perceptual thresholds in epiretinal prostheses. Invest. Oph. Vis. Sci. 49, 2303–2314 (2008)

[21] D. L. Villarreal et al., "Biomimetic Stimulating Array for Single Localized Stimulation in Visual Prosthesis," Int J of Comp & Neural Eng (IJCNE), vol. 4, no. 3, pp. 76-90, 17 October 2017

[22] Kasi et al., "Simulation of epiretinal prostheses - Evaluation of geometrical factors affecting stimulation thresholds," J of NeuEng and Rehab, vol. 8, no. 1, pp. 1-10, 2011.

[23] G. K. Moghaddam et al., "Performance optimization of current focusing and virtual electrode strategies in retinal implants," vol. 117, no. 2, pp. 334-342, November 2014.

[24] H. Kasi et al., "Simulations to study spatial extent of stimulation and effect of electrode–tissue gap in subretinal implants," Medical Engineering & Physics, vol. 33, no. 6, pp. 755-763, 2011.

[25] K. Loizos et al., "A multi-scale computational model for the study of retinal prosthetic stimulation," IEEE Med & Bio Society 2014, 2015.

[26] M Abramian et al. Computational model of electrical stimulation of a retinal ganglion cell with hexagonally arranged electrodes. EMBS (2012)

[27] D. L. Villarreal et al. Spatial Visual Perceptions by Means of Simulated Prosthetic Vision. In: VIII La Ame Conf on Biom Eng, XLII Nat Conf Biom Eng. IFMBE Proc, vol 75. Springer (2020)

[28] G Roessler, et al. Angiographic findings following tack fixation of a wireless epiretinal retina implant device in blind RP patients. Graefes Arch Clin Exp Ophthalmol. 2011 Sep;249(9):1281-6.

[29] E. Cohen et al., "Optical coherence tomography imaging of retinal damage in real time under a stimulus electrode," J Neu Eng vol. 8, no. 5, Sep 2011